Magnetite Nanoparticles Anchored to Crystalline Silicon Surfaces

Fabrizio Cattaruzza, Dino Fiorani, Alberto Flamini,* Patrizia Imperatori, Guido Scavia, Lorenza Suber,* and Alberto M. Testa

CNR−Istituto di Struttura della Materia, PO Box 10, 00016 Monterotondo St, Italy

Alessio Mezzi

CNR−Istituto per lo Studio dei Materiali Nanostrutturati, PO Box 10, 00016 Monterotondo St, Italy

Giovanni Ausanio

INFM−Dipartimento Scienze Fisiche Università di Napoli, Napoli, Italy

William R. Plunkett

Center for Advanced Materials Processing, Clarkson University, Potsdam, New York 13699-5814

Received January 31, 2005. Revised Manuscript Received April 4, 2005

Magnetite nanoparticles of 5 nm mean diameter, coated with 10-undecynoic acid, have been anchored to crystalline Si(100) surfaces via the hydrosilylation reaction at 180 °C. The iron content in the sample (0.54 ± 0.05 μg/cm^2) has been determined by atomic absorption analysis. The sample has been further characterized by X-ray photoelectron spectroscopy, field emission scanning, scanning-tunneling, and atomic force (AFM) microscopies. The thermal anchoring does not alter the morphology of the nanoparticles, causing only a slight oxidation of their surfaces. However, a second layer of nanoparticles was also formed, covering about 50% of the surface. The magnetic properties were studied using a SQUID magnetometer. ZFC (zero-field cooled) and FC (field cooled) curves were obtained in the 5−300 K temperature range. The ZFC curve shows a rounded maximum at $T_{max} \sim 20$ K. A hysteretic magnetization cycle was also observed at 5 K with associated magnetization saturation and coercitivity values of 40 emu/g and 160 Oe, respectively. The magnetic behavior of the sample was found to be typical of an assembly of noninteracting (or very weakly interacting) super-paramagnetic particles.

Introduction

The covalent assembling of magnetic nanoparticles on the surface of an appropriate substrate is a very appealing research topic, as the resulting materials are relevant for fundamental studies [1,2] as well as for a number of technological applications based on nanostructured architectures.[3,4] This is particularly true when the solid substrate is unoxidized crystalline silicon because this material is considered to be almost the ideal substrate in this field, owing to the uniformity and homogeneity of its surface at the nanometer scale.[5,6] Generally, the attachment of nanoparticles to a surface needs special linkers, such as α,ω-heterobifunctional molecules, able to act as bridges between the surface and the nanoparticles.[7] It has been demonstrated that linear-chain 1-carboxylic acids with unsaturated ends are suitable bridging molecules for certain applications on unoxidized silicon substrates. These molecules bind to silicon surfaces through a covalent Si−C bond after the hydrosilylation reaction. Then, the free carboxylic end group, because of its rich and versatile chemistry, can be utilized in a subsequent step[8−11] as a handle to bind other species to the surface, imparting it with additional properties to be exploited in the design of silicon based electronic devices.

Some of us have recently prepared and characterized carboxylic acid terminated planar crystalline silicon surfaces, obtained from the reaction in solution between hydrogenated silicon and 10-undecynoic acid, HC≡C−$(CH_2)_8$COOH (Scheme 1, A).[12] For the stated considerations, these surfaces, after functionalization with magnetic nanoparticles, could be

* Corresponding authors. E-mail: (A.F.) alberto.flamini@ism.cnr.it; (L.S.) lorenza.suber@ism.cnr.it.

(1) Thiaville, A.; Miltat, J. *Science* **1999**, *284*, 1939−1940.
(2) Cornia, A.; Fabretti, A. C.; Pacchioni, M.; Zobbi, L.; Bonacchi, D.; Caneschi, A.; Gatteschi, D.; Biagi, R.; Del Pennino, U.; De Renzi, V.; Gurevich, L.; Van der Zant, H. S. J. *Angew. Chem.* **2003**, *115*, 1683−1686.
(3) Palacin, S.; Hidber, P. C.; Bourgoin, J. P.; Miramond, C.; Fermon, C.; Whitesides, G. M. *Chem. Mater.* **1996**, *8*, 1316−1325.
(4) Zhong, Z.; Gates, B.; Xia, Y. *Langmuir* **2000**, *16*, 10369−10375.
(5) Hersam, M. C.; Guisinger, N. P.; Lyding, J. W. *Nanotechnology* **2000**, *11*, 70−76.
(6) Yin, H. B.; Brown, T.; Greef, R.; Wilkinson, J. S.; Melvin, T. *Microelectron. Eng.* **2004**, *73−74*, 830−836.
(7) Yamanoi, Y.; Yonezawa, T.; Shirahata, N.; Nishihara, H. *Langmuir* **2004**, *20*, 1054−1056.
(8) Sieval, A. B.; Demirel, A. L.; Nissink, J. W. M.; Linford, M. R.; van der Mass, J. H.; de Jeu, W. H.; Zuilhof, H.; Sudhölter, E. J. R. *Langmuir* **1998**, *14*, 1759−1768.
(9) Boukherroub, R.; Wayner, D. D. M. *J. Am. Chem. Soc.* **1999**, *121*, 11513−11515.
(10) Strother, T.; Cai, W.; Zhao, X.; Hamers, R. J.; Smith, L. M. *J. Am. Chem. Soc.* **2000**, *122*, 1205−1209.
(11) Wei, F.; Sun, B.; Guo, Y.; Zhao, X. S. *Biosens. Bioelectron.* **2003**, *18*, 1157−1163.
(12) Cattaruzza, F.; Cricenti, A.; Flamini, A.; Girasole, M.; Longo, G.; Mezzi, A.; Prosperi, T. *J. Mater. Chem.* **2004**, *14*, 1461−1468.

10.1021/cm050231a CCC: $30.25
Published on Web 05/20/2005

Scheme 1

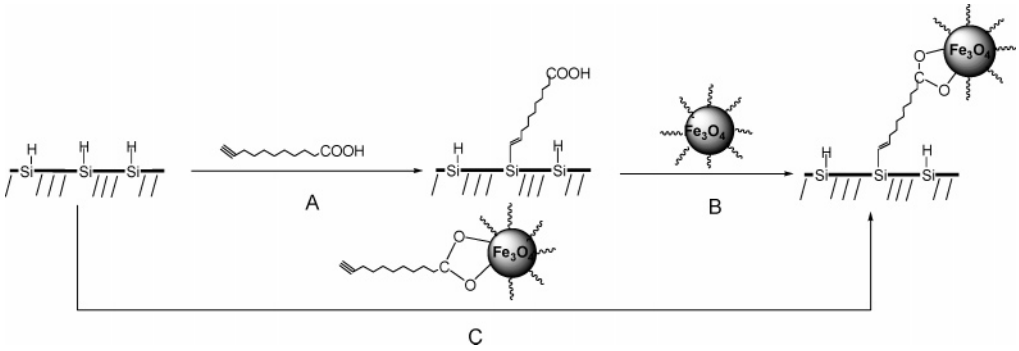

of great potential for future advanced magnetic applications. Among the most important magnetic species to be considered in this context are magnetite nanoparticles that, to the best of our knowledge, have not yet been anchored to unoxidized silicon surfaces. Indeed, magnetite (Fe_3O_4) is ferrimagnet (the Curie temperature is 860 K)[13] crystallizing in the spinel structure, with a single $3d^{\downarrow}$ electron hopping among the $3d5^{\uparrow}$ cores on octahedral sites. Band calculations predict the conduction electrons to be fully spin polarized[14,15] in such a way that magnetite is half metallic but with a strong tendency to form polarons below T_c, and the conductivity shows a small activation energy. Its half metallic character makes it a very interesting candidate to be exploited in sources and analyzers of completely spin-polarized electrons in spin electronics applications.[16−18]

After the report on iron oxide ultrafine particles capped by the carboxylate group of an aliphatic acid,[19] we promptly realized that magnetite nanoparticles might be anchored to silicon surfaces, utilizing 10-undecynoic acid as the cross-linker between the surface and the nanoparticles, through the routes, either A + B or C, as sketched in Scheme 1.

In this paper, we report on anchoring magnetite nanoparticles to a crystalline silicon substrate through route C and on the microstructural and magnetic properties of the final material.

Experimental Procedures

Materials and Synthesis Procedures. All the syntheses were carried out using airless procedures in an N_2-(g)-purged Dry-Box (Braun) or using standard preparative Schlenk line procedures.

Commercially available reagents were used. Absolute ethanol, hexane, mesitylene, benzyl ether (99%), 1,2-hexadecanediol (97%), oleic acid (90%), oleylamine (>70%), iron(II)-acetylacetonate, and 10-undecynoic acid (95%) were purchased from Aldrich Chemical Co. and used as received. Mesitylene was refluxed and then distilled at atmospheric pressure under dinitrogen over sodium lumps and stored in the Dry-Box. Silicon wafers of 2.5 cm diameter and 250 μm thickness, p-Si, boron-doped, double-side polished, 0.01 Ω cm resistivity, (100) orientation were purchased from Siltronix. Silicon was hydrogenated in solution on treatment with aqueous HF, after a preliminary cleaning and oxidation step, according to a procedure reported elsewhere.[12] Briefly, silicon wafers were first washed in boiling 1,1,2-trichloroethane for 10 min, then in methanol at room temperature with sonication for 5 min, oxidized in H_2O_2/HCl/H_2O (2:1:8) at 80 °C for 15 min, rinsed copiously with deionized water, etched with 10% aqueous HF for 10 min, rinsed with water again, and finally dried under a stream of N_2.

Preparation and Characterization of Magnetite Nanoparticles of 5 nm Diameter, Coated by 10-Undecynoic Acid. $Fe(acac)_2$ (2 mmol), 1,2-hexadecanediol (10 mmol), oleic acid (6 mmol), oleylamine (6 mmol), and benzyl ether (20 mL) were mixed and magnetically stirred under nitrogen. The reaction flask was immersed in an oil bath at 200 °C for 30 min, the oil bath temperature was then raised to 220 °C, and the reaction flask was heated for another 30 min. The black−brown mixture was cooled to room temperature by removing the heat source. Ethanol (40 mL) was added to the mixture. A black precipitate was separated via centrifugation. The product was then dissolved in 50 mL of hexane containing oleic acid (0.05 mL) and oleylamine (0.05 mL). Centrifugation (8000 rpm, 10 min) was used to remove any undispersed residue. Ethanol was then added to the dispersion, the resulting mixture was centrifuged, and the solid product was dispersed again in hexane. This procedure was repeated twice to remove any excess oleic acid. The coupling of 10-undecynoic acid to the nanoparticles was then attained after an exchange reaction in a colloidal solution, as follows. The product of the previous step, dispersed in 40 mL of hexane containing 10-undecynoic acid (550 mg, 3 mmol), was heated under nitrogen at 60 °C and mechanically stirred overnight. It was cooled to room temperature and, after the addition of 40 mL of ethanol, centrifuged. The black product was dispersed in hexane and centrifuged to remove any undispersed residue. Ethanol was added to the dispersion, the mixture was centrifuged, and the solid product was dispersed again in hexane. This procedure was repeated twice to remove any excess undecynoic acid. Finally, the product was dried overnight under vacuum and collected. Analysis: found: C, 14.18; H, 2.01%. Calcd. for $(Fe_3O_4)_{3.2}(C_{11}H_{20}O_2)$: C, 14.19; H, 2.16%. By assuming this formula, the yield of the isolated product was 48%, based on $Fe(acac)_2$.

IR: 3296 (w, H−CC), 2921 and 2857 (m, H−C), 2117 (w, HC≡C), 1533 and 1432 (s, COO^-). Differential thermal analyses (DTA) in air show an exothermic peak at 250 °C. This product was further characterized by X-ray diffraction (XRD) analysis with results reported in the next section.

Anchoring of Magnetite Nanoparticles to Crystalline Silicon Surfaces. The magnetite nanoparticles, covered with 10-undecynoic acid (158 mg), were dissolved under N_2 in mesitylene (10 mL) forming a dark brown solution. A freshly etched silicon wafer was

(13) Glasser, M. L.; Milford, F. J. *Phys. Rev.* **1963**, *130*, 1783−1789.
(14) Yanase, A.; Siratori, K. *J. Phys. Soc. Jpn.* **1984**, *53*, 312−317.
(15) Yanase, A.; Hamada, N. *J. Phys. Soc. Jpn.* **1999**, *68*, 1607−1613.
(16) Bobo, J. F.; Gabillet, L.; Bibes, M. *J. Phys. Condens. Matter* **2004**, *16*, S471−S496.
(17) Parkin, S.; Jiang, X.; Kaiser, C.; Panchula, A.; Roche, K.; Samant, M. *Proc. IEEE* **2003**, *91*, 661−680.
(18) Sih, V. A.; Johnston-Halperin, E.; Awschalom, D. *Proc. IEEE* **2003**, *91*, 752−760.
(19) Bourlinos, A. B.; Simopoulos, A.; Petridis, D. *Chem. Mater.* **2002**, *14*, 899−903.

immersed in this solution. The mixture was heated at 180 °C for 2 h in a stoppered glass container filled with N_2. The silicon sample was cleaned by sonication in air 3 times with different solvents for 5 min each (mesitylene, acetonitrile, methanol) and dried in a stream of N_2. The amount of iron present on the silicon surface of the final samples was determined by atomic absorption spectroscopy as follows. Three silicon wafers, equivalent to an active surface area 30.62 cm^2, were functionalized with magnetite nanoparticles as described previously. Then, the silicon wafers were treated with concentrated HNO_3 (4 mL) at reflux for 3 h. After this treatment, the nanoparticles were completely detached from the surface as revealed by iron XPS (see infra). This solution was transferred to a 10 mL volumetric flask to which water was added (Carlo Erba Water Plus, 3 × 2 mL). Standard water iron solutions, in the concentration range of 0−2 ppm, were prepared and measured. The resulting calibration plot was linear ($y = 0.11192x$) with an associated correlation index equal to 0.9996. By using this plot, the 10 mL solution was measured, and the iron concentration was determined (i.e., 1.64 ± 0.15 ppm/ mL, equivalent to 9.5 ngram-atoms/cm^2). Further characterization was performed with X-ray photoelectron spectroscopy (XPS), scanning probe microscopies, and magnetic measurements with results reported in the next section.

Physical Techniques. DTA analysis was performed in air with a DuPont 950 apparatus. A Shimadzu AA-6300IR instrument was used for atomic absorption iron analysis. IR measurements were performed with a Perkin-Elmer 16F PC FT spectrometer on KBr pellets (0.75% w/w); the stretching frequencies (ν/cm^{-1}) of the absorption maximum of the most significant bands are given. FE−SEM (field emission scanning electron microscopy) images were obtained with a JEOL 7400F. Scanning tunneling microscopy (STM) characterization was carried out with a commercial STM−UHV system (WA tech). The typical tunneling parameters are tip−sample voltage = 2−3 V and tunneling current = 0.05−0.08 nA. Atomic force microscopy (AFM) investigations were performed with Digital Instruments nanoscope IIIa, equipped with a sharpened silicon tip with a radius less than 5 nm. The images of the surface profiles were obtained by operating the AFM in the tapping mode, with a scan size of 1000 nm and a rate of 2 Hz. XRD measurements were performed on a Seifert XRD 3000 powder diffractometer in the 2θ range 25−85°, using CuKα radiation ($\lambda = 1.5418$ Å). Magnetic measurements were performed by a commercial SQUID magnetometer operating between 2 and 400 K, with a maximum magnetic field of 55 kOe. The XPS studies were performed in an ESCALAB MkII (VG Scientific) instrument, using the AlKα line as a source ($h\nu = 1486.6$ eV) and a five-channeltron as a detection system. Photoelectrons were probed at a takeoff angle of 90°, while the analyzer was opened with a constant pass energy of 20 eV. The pressure from residual gases never exceeded 1 × 10^{-8} mbar in the analysis chamber during the measuring time. The linearity of the binding energy (BE) scale was calibrated according to the procedures proposed by Seah and Smith.[20] Following this calibration, both the accuracy and the reproducibility of measurements were found to be within ±0.1 eV. To compensate for charging phenomena, measured BEs were referenced to that of a C 1s peak (resulting from carbonaceous contamination adventitiously adsorbed onto the surface), taken as lying at 285.0 ± 0.1 eV.

Results and Discussion

The magnetite nanoparticles have been anchored to the silicon surface with the intervening undecynoic acid as cross-linker between the particles and the surface. In particular, they are anchored through a coordination bond to the carboxylate group of the acid that, in turn, is attached to the surface via a covalent C−Si bond. To accomplish this, we followed a multistep procedure, consisting of (1) the preparation of magnetite nanoparticles covered by oleic acid, (2) the exchange between oleic acid and undecynoic acid on the surface of the nanoparticles, and finally, (3) the anchoring these particles, covered by undecynoic acid, to the silicon surface.

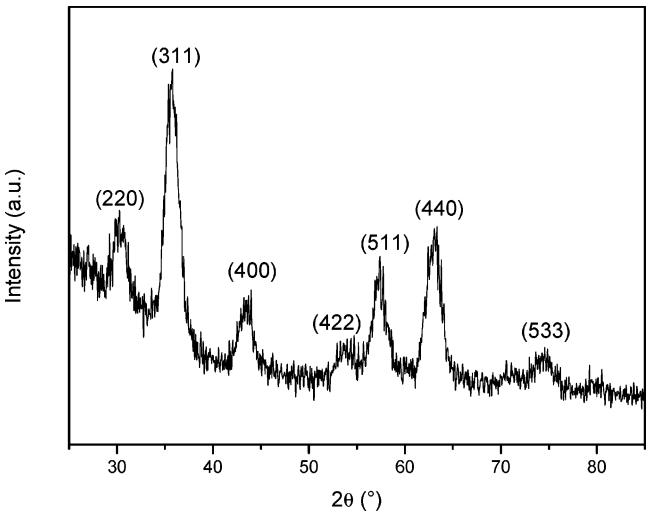

Figure 1. X-ray diffraction pattern of magnetite (Fe_3O_4) powder.

Preparation of the Samples. Magnetite nanoparticles, covered by oleic acid, were prepared by applying a modified method of the literature.[21] Modifications introduced consisted of starting from $Fe(acac)_2$ instead of $Fe(acac)_3$ to hinder as much as possible the growth of the oxidized phase maghemite (γ-Fe_2O_3) during the formation of magnetite and using a 50 °C lower reaction temperature to slightly increase the particle size. Then, oleic acid was exchanged with undecynoic acid. A complete exchange occurred on the surface of the magnetite particles. In fact, CHN elemental analyses of magnetite nanoparticles covered by 10-undecynoic acid showed it to be a nitrogen-free product, in agreement with the formula $(Fe_3O_4)_{3.2}(C_{11}H_{20}O_2)$. It should be noted that the measured H/C atomic ratio is 1.69, which compares well with the theoretical value of 1.64 for undecynoic acid, whereas the theoretical value for oleic acid is 1.89. IR spectra show the absorption bands characteristic of ionized undecynoic acid. The XRD pattern (Figure 1) provides additional structural information on the sample. The positions of all diffraction peaks match those of magnetite.[22] The peak broadening can be attributed mainly to the small crystallite size of the powder, which is directly related to the decrease in the particle size. The peaks, after a correction for the instrumental broadening, were fitted with a pseudo-Voigt profile shape function. The full width at half-maximum (fwhm) and the mixing parameter (η) values, resulting from the fitting procedure, were used as input for the program

(20) Seah, M. P.; Smith, G. C. In *Practical Surface Analysis*, Vol. 1; Briggs, D., Seah, M. P., Eds.; J. Wiley & Sons: Chichester, UK, 1990; p 531.

(21) Sun, S.; Zeng, H.; Robinson, D. B.; Raoux, S.; Rice, P. M.; Wang, S. X.; Li, G. *J. Am. Chem. Soc.* **2004**, *125*, 273−279.

(22) (JPCDS 19-0629). It is to note that, due to the proximity of the peaks of the oxidized phase (maghemite, γ-Fe_2O_3), the presence of maghemite cannot be, on the basis of only XRD data, completely excluded.

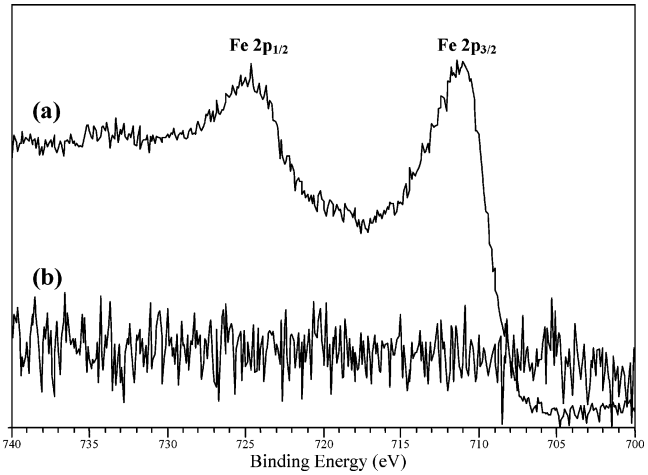

Figure 2. Fe 2p region XPS spectra of the Si (100) surfaces covered with magnetite nanoparticles before (a) and after (b) the removal of the nanoparticles.

BREADTH,[23] to determine the volume weighted mean crystallite size and its distribution function, according to the double-Voigt method.[24] An average crystallite size of 5.3 ± 1.2 nm was estimated. Furthermore, DTA analysis shows a peak attributable to the expected oxidation phase change from magnetite (Fe_3O_4) to maghemite (γ-Fe_2O_3).[25]

In the final step, the magnetite nanoparticles coated with undecynoic acid were anchored to the silicon surface through a stable covalent C−Si bond via the well-known hydrosilylation reaction as reported in the literature for the silicon thermal functionalization with terminal alkynes in organic solutions.[26,27] During the reaction workup, particular attention was paid to the washing procedure to remove any physisorbed species. To this end, stringent rinsing in ultrasonic baths of various solvents was applied.

The surface chemical composition of the sample was studied by means of XPS, and a typical Fe 2p spectrum is shown in Figure 2. The identification of iron oxidic species can be derived from the binding energy (BE) of the Fe 2p3/2 component and from the satellite shake-up structure accompanying the (3/2, 1/2) spin−orbit split Fe 2p spectrum. We conclude that our sample consists of an Fe_3O_4-like phase since the relevant Fe 2p3/2 component lies at BE = 710.9 eV and no sizable satellite structure is observed.[28−30] (A satellite signal lying ∼6 or ∼8 eV to the high-BE side of each main component would be observed had FeO or Fe_2O_3 been present, respectively.)

In addition, the iron content in the sample (a) was determined by atomic absorption in a water solution after completely removing the nanoparticles from the silicon sample with concentrated HNO_3 at reflux. The effectiveness of this treatment was ascertained, again, by XPS analysis (Figure 2). The resulting iron value, 0.54 ± 0.05 μg/cm^2, corresponds to a densely packed magnetite particle monolayer covering approximately 50% of the silicon substrate, assuming a mean particle diameter of 5 nm. These results were consistent with our earlier findings,[12] and with those of other authors,[31] which indicated that functionalization reactions in solution on silicon surfaces are not complete.

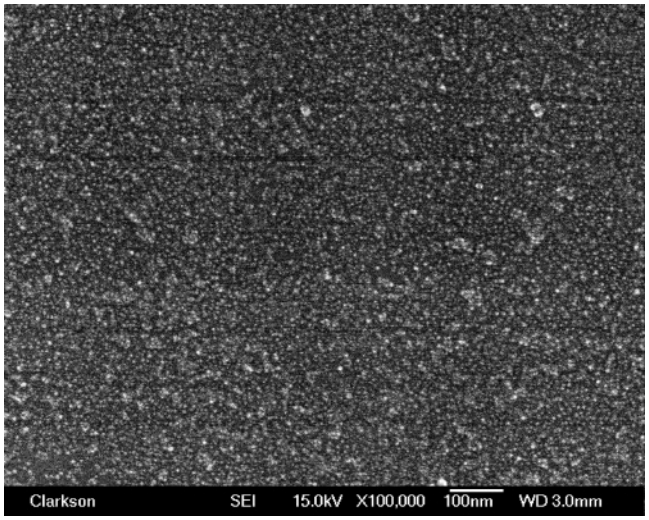

Figure 3. FE−SEM micrograph of a Si (100) crystalline surface (1.2 × 0.87 μm) covered with magnetite particles.

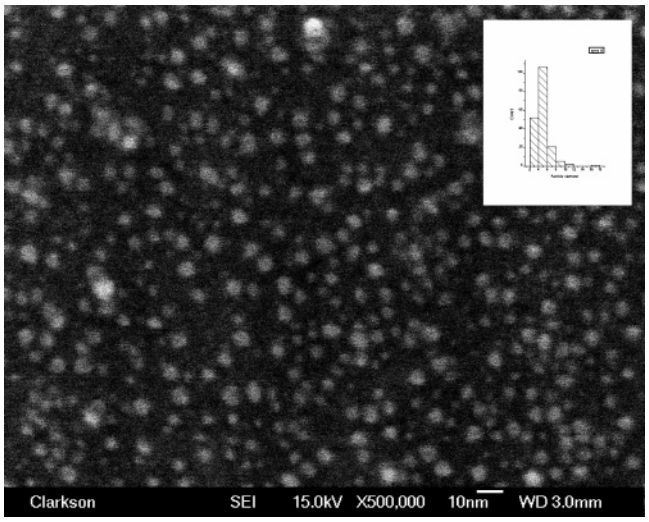

Figure 4. FE−SEM micrograph of a Si(100) crystalline surface (120 × 87 nm) covered with magnetite particles. The inset shows the size distribution histogram obtained measuring all the particles of the image (see text).

Morphology Characterization. The morphology of the sample was characterized by field emission-scanning, scanning-tunneling, and atomic force-microscopies.

FE−SEM investigations show well-distributed, almost spherical particles (Figures 3 and 4). The size distribution obtained measuring 195 particles in Figure 5 is fitted to a log-normal function centered at 5 ± 1 nm. Figure 5 shows a comparison between the size distribution obtained by FE−

(23) http://www.boulder.nist.gov/div853/balzar/breadth.htm.
(24) Balzar, D.; Ledbetter, H. *J. Appl. Crystallogr.* **1993**, *26*, 97−103.
(25) Cornell, R. M.; Schwertmann, U. *The Iron Oxides*; Wiley-VCH: Weinheim, 1996.
(26) Bateman, E. J.; Eagling, R. D.; Worral, D. L.; Horrocks, B. R.; Houlton, A. *Angew. Chem., Int. Ed. Engl.* **1998**, *37*, 2683−2685.
(27) Sieval, A. B.; Opitz, R.; Maas, H. P. A.; Schoeman, G. M.; Meijer, G.; Vergeldt, F. J.; Zuilhof, H.; Sudhölter, E. J. R. *Langmuir* **2000**, *16*, 10359−10368.
(28) Brundle, C. R.; Chuang, T. J.; Wandelt, K. *Surf. Sci.* **1977**, *68*, 459−468.
(29) McIntyre, N. S.; Zetaruk, D. G. *Anal. Chem.* **1977**, *49*, 1521−1529.
(30) McIntyre, N. S.; Chan, T. C. In *Practical Surface Analysis*, Vol. 1; Briggs, D., Seah, M. P., Eds.; J. Wiley & Sons: Chichester, UK, 1990.
(31) Cerofolini, G. F.; Galati, C.; Reina, S.; Renna, L. *Mater. Sci. Eng. C* **2003**, *23*, 253−257.

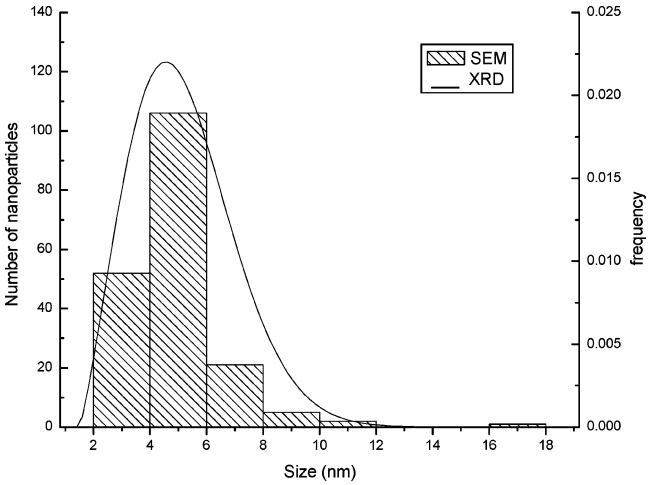

Figure 5. Comparison between the histogram of nanoparticle size distribution as obtained from SEM measurements and the log-normal distribution size inferred from XRD data analysis.

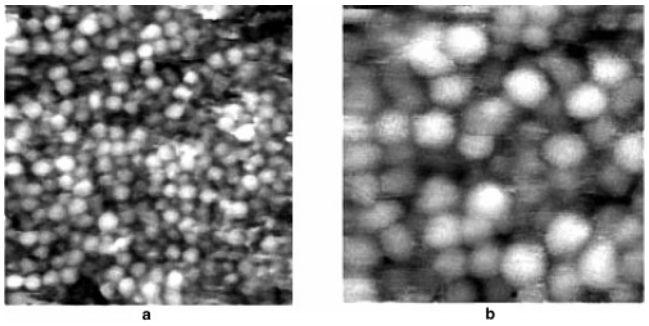

Figure 6. STM images of the magnetite nanoparticles attached to the Si-(100) surface at different scales. (X,Y range = 100 and 45 nm for panels a and b, respectively).

SEM measurements on the magnetite particles attached to the silicon surface and the log-normal distribution calculated from XRD data on the pristine particles. Noticeably, similar particle size and size distribution were obtained. We conclude, then, that the thermal anchoring of the nanoparticles to the surface does not alter their morphology.

STM images (Figure 6) show a homogeneous distribution of almost spherical particles with typical dimensions of 4−6 nm. The particle close packing indicates that the organic molecules covering the nanoparticles are efficient ligands for them. Moreover, areas in which nanoparticles form a second layer on top of the first one are also visualized; the different gray tones of the images indicate that the grains are distributed on the surface at two different heights with respect to the silicon substrate.

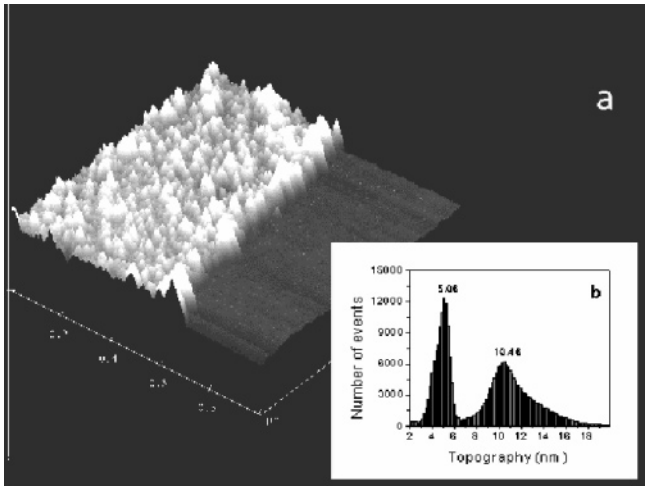

Figure 7. (a) AFM 3-D view of the sample, 1 × 1 μm. (b) Statistical height histogram of AFM image 7a.

To account for this, a reliable route leading to the formation of the double layer, interconnected by covalent bonds, has been proposed and is depicted in Scheme 2.

Excluding any nonspecific interactions and given the stringent washing conditions during the preparation of the samples as pointed out previously, we reason that during the thermal functionalization of the silicon surface and after the growth of the monolayer to some extent, a magnetite nanoparticle in solution, capped by undecynoic acid, might react either with hydrogenated silicon contributing to the monolayer (1) or with other nanoparticles, already cast in the monolayer, so forming a double layer (2). In the latter case, the reaction type at work could be the terminal alkyne dimerization, occurring between two 10-undecynoic acid surfactant molecules, belonging to two different nanoparticles, one bonded to silicon (e.g., Y−C≡CH) and the other one dispersed in solution (e.g., Z−HC≡C). This is a well-known reaction in alkyne chemistry, which yields vinylacetylenes: Y−C≡CH + HC≡C−Z → Y−C≡CH−CH═CH−Z.[32]

AFM images also indicate a particle lay-out analogous to that observed by STM. Interestingly, during this investigation, some particle-free silicon gaps, adjacent to the nanoparticle double layers, came into focus, displaying the line of demarcation along which the two areas meet (Figure 7a). So, we had the opportunity to measure the individual layer thickness at the boundary line between the bare Si substrate and the layer of deposited nanoparticles. The height distribution evaluated from statistical analysis of the AFM image in Figure 7a clearly shows two maximum peaks (Figure 7b).

Scheme 2

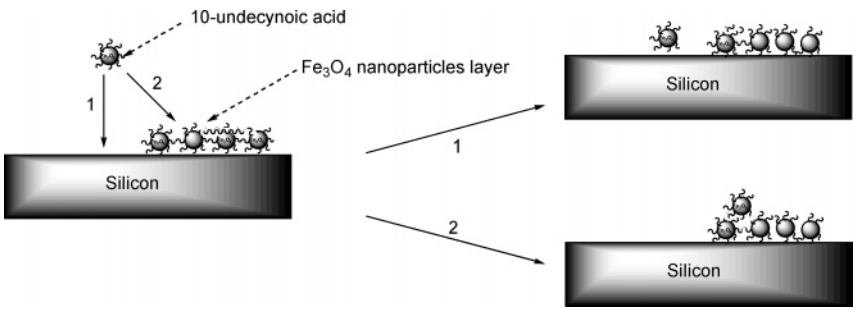

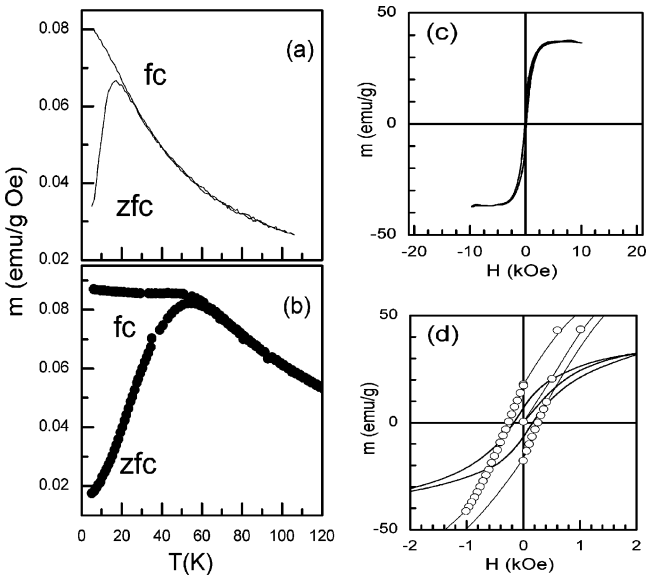

Figure 8. Magnetization as a function of temperature: (a) Fe_3O_4 particles attached to silicon, $H_a = 100$ Oe (solid line). (b) Pristine Fe_3O_4 powder, $H_a = 20$ Oe (symbols). (c) Magnetization vs applied magnetic field at 5 K. (d) Magnification of the field range −1 kOe/+1 kOe: silicon attached particles (solid line) and pristine particles (open symbols).

The first peak centered at 5.0 nm is related to one layer of silicon attached nanoparticles, while the second peak centered at 10.5 nm is related to nanoparticles deposited on the first layer. Because the peak area ratio is 1, as shown in Figure 7b, the surface covered by one nanoparticle layer is 2 times larger than the surface covered by the second layer.

Magnetic Measurements. The temperature dependence of the magnetization measured by means of a commercial SQUID magnetometer is shown in Figure 8a for particles anchored to the Si surface. The curve marked as ZFC (zero-field cooled) was obtained by first cooling the system in zero magnetic field from 300 to 5 K; the magnetic field was then applied, and the magnetization was measured while increasing the temperature. The curve marked as FC (field cooled) was obtained by measuring the magnetization while the temperature was decreased in the same magnetic field. Both curves exhibit the main features of super-paramagnetic systems. Namely, the ZFC curve shows a rounded maximum at $T_{max} \sim 20$ K, whereas the FC branch continues to increase with decreasing temperature; moreover, the ZFC and FC branches of the magnetization curve overlap at a temperature slightly larger than T_{max}, with a temperature dependence of a Curie−Weiss type. The temperature behavior of the FC branch should reflect the non- (or very weakly) interacting character of the particle assembly.[33]

In such a case, the Neel−Brown law for the relaxation time of the particle moment $K_a = 25kT_b/V$[34] can be used. T_b is the blocking temperature, defined as the temperature at which the relaxation time of the particle moment is on the order of the experimental time window (ca. 100 s for macroscopic magnetic measurements), V is the particle volume, and K_a can be deduced from the Arrhenius law replacing V with the mean particle volume $\langle V \rangle$ and T_b with the mean blocking temperature $\langle T_b \rangle$. Because of the log-normal particle size distribution, $\langle T_b \rangle = T_{max}/c$, where $c = 1.5$.[35] It turns out that $K_a = 6 \times 10^5$ erg/cm^3. By contrast, for pristine nanoparticles in a powder form (Figure 8b), the ZFC curve of the magnetization versus temperature shows a rounded maximum at T_{max} ca. 55 K, and the FC curve displays a flattening as the temperature decreases. The higher T_{max} value (reflecting an increase of the effective anisotropy energy barrier) and the behavior of the FC magnetization is usually ascribed to the presence of interparticle interactions[33] to which the associated energy is much higher than the single particle anisotropy energy, unlike for Fe_3O_4 particles attached to the Si surface. An intermediate behavior ($T_{max} = 26$ K; tendency to flattening of the FC magnetization below T_{max}), revealing the existence of non-negligible interparticle interactions, was observed for particles deposited on Si, weakly bonded to the surface. The magnetization cycle at 5 K of silicon attached nanoparticles is shown in Figure 8c. The magnetization saturation value is 40 emu/g, much lower than the magnetite bulk value (92 emu/g).[36] Spin canting and disorder at the particle surface, associated with the breaking of crystal symmetry, could be responsible for such a reduction. The low field region of the magnetization cycles for silicon attached and pristine particles is shown in Figure 8d. The difference in coercivity between the two samples (260 Oe for the pristine sample; 160 Oe for the silicon attached particles) should be mainly due to the different surface state of the particles, due to covalent bonds with the Si substrate depending on the actual roughness profile of the sample (incomplete particle double layering).

Conclusions

We have demonstrated that magnetite nanoparticles can be anchored to unoxidized crystalline silicon surfaces with the aid of a carboxylic acid as the cross-coupling agent via a thermal reaction. Large islands of nanoparticle double layers were also concomitantly formed indicating that multiparticle layers can probably also be obtained by properly tuning the reaction time. By contrast, we envisage reaction B in Scheme 1 for the formation of a particle single monolayer. This reaction is, in fact, expected to be carried out at low temperatures to avoid the terminal alkyne dimerization, responsible for the double and eventually multilayer formation. The preparation methods reported, of chemically attaching the particles to the Si substrate and tailoring the particle layer formation, are therefore well-suited for obtaining nanomagnetic materials with optimized magnetic properties for spintronics applications.

CM050231A

(32) Smith, M. B.; March, J. *March's Advanced Organic Chemistry*; Wiley-Interscience: New York, 2001; p 1020.
(33) Dormann, J. L.; Fiorani, D.; Tronc, E. *Adv. Chem. Phys.* **1997**, *98*, 283−294.
(34) (a) Neel, L. *Ann. Geophys.* **1949**, *5*, 99. (b) Brown, W. F. *Phys. Rev.* **1963**, *130*, 1677−1686.
(35) Pankhurst, Q. A.; Ucko, D. H.; Fernandez Barquin, L.; Garcia Calderon, R. *J. Magn. Magn. Mater.* **2003**, *266*, 131−141.
(36) Popplewell, J.; Sakhnini, L. *J. Magn. Magn. Mater.* **1995**, *149*, 72−78.